PROCEEDINGS OF THE ROYAL SOCIETY A MATHEMATICAL, PHYSICAL & ENGINEERING SCIENCES

A thermal analysis of the operation of microscale, inorganic light-emitting diodes

Chaofeng Lu, Yuhang Li, Jizhou Song, Hoon-Sik Kim, Eric Brueckner, Bo Fang, Keh-Chih Hwang, Yonggang Huang, Ralph G. Nuzzo and John A. Rogers

Proc. R. Soc. A 2012 **468**, 3215-3223 first published online 15 June 2012
doi: 10.1098/rspa.2012.0225

PROCEEDINGS OF THE ROYAL SOCIETY A

CrossMark click for updates

Proc. R. Soc. A (2012) **468**, 3215–3223
doi:10.1098/rspa.2012.0225
Published online 15 June 2012

A thermal analysis of the operation of microscale, inorganic light-emitting diodes

By Chaofeng Lu[1,2,3,†], Yuhang Li[2,3,4,†], Jizhou Song[5,*], Hoon-Sik Kim[6], Eric Brueckner[7], Bo Fang[4], Keh-Chih Hwang[8], Yonggang Huang[2,3,*], Ralph G. Nuzzo[7] and John A. Rogers[6,7]

[1]*Department of Civil Engineering and Soft Matter Research Center, Zhejiang University, Hangzhou 310058, People's Republic of China*
[2]*Department of Civil and Environmental Engineering, and* [3]*Department of Mechanical Engineering, Northwestern University, Evanston, IL 60208, USA*
[4]*School of Astronautics, Harbin Institute of Technology, Harbin 150001, People's Republic of China*
[5]*Department of Mechanical and Aerospace Engineering, University of Miami, Coral Gables, FL 33146, USA*
[6]*Department of Materials Science and Engineering, and* [7]*Department of Chemistry, University of Illinois, Urbana, IL 61801, USA*
[8]*Department of Engineering Mechanics, Tsinghua University, Beijing 100084, People's Republic of China*

An analytical model is developed to study the thermal properties of microscale, inorganic light-emitting diodes (μ-ILEDs) with ultra-thin geometries and layouts. The predicted surface and μ-ILED temperatures agree well with experiments and finite-element simulations. A simple scaling law is obtained for the normalized μ-ILED temperature versus the normalized μ-ILED size. This study provides a theory to guide the design of layouts that minimize adverse thermal effects on the performance of μ-ILEDs not only for solid-state lighting but also for applications integrating μ-ILED devices on complex/soft substrate as are currently of interest in optogenetics and other emerging areas in biology.

Keywords: thermal analysis; solid-state lighting; gallium nitride

1. Introduction

Indium gallium nitride-based (InGaN) light-emitting diodes (LEDs) offer combined characteristics in cost, efficiency and lifetime, which make them attractive for broad classes of application in solid-state lighting (Schubert & Kim 2005; Tsao *et al.* 2010). Conventional routes to LEDs involve epitaxial growth of active materials followed by wafer dicing and pick-and-up robotic manipulation into individually packaged components that are then interconnected by bulk wire bonding and mounted on millimetre-scale heat sinks for thermal

*Authors for correspondence (jsong8@miami.edu; y-huang@northwestern.edu).

†These authors contributed equally to this study.

Received 13 April 2012
Accepted 17 May 2012

management. Although suitable for many uses, such designs do not allow practical realization of potentially valuable engineering options, such as those that involve large collections of small devices or unusual substrates. Kim *et al.* (2011) recently reported schemes that avoid these limitations by use of advanced methods in epitaxial lift-off and deterministic assembly. The result is a realistic route to classes of LEDs that can be much thinner and smaller than those accessible using conventional procedures, in which interconnection is accomplished with thin-film metallization and photolithography. The process begins with the growth of InGaN epitaxial material on silicon wafers with (111) orientation followed by the definition of arrays of individual LEDs with microscale dimensions (down to approx. $25 \times 25\,\mu m$), referred to as microscale inorganic LEDs (μ-ILEDs). Anisotropic wet chemical etching of the underlying silicon releases devices for transfer printing onto foreign substrates (e.g. glass or plastic). A photodefinable layer of benzocyclobutene (BCB; figure 1*a*) provides a top layer encapsulant that leaves the p- and n-type ohmic contacts (figure 1*a*) of each device exposed. Depositing and patterning of a metal layer (figure 1*a*) yields electrical interconnects that serve simultaneously as heat spreaders. Figure 1*a* shows the layouts of a single μ-ILED on a glass substrate where the small gap within the metal layer isolates p- and n-contacts to avoid short circuit. This gap also serves as a good approximation of the μ-ILED temperature because the BCB layer on the μ-ILED is very thin (approx. 1 μm). The cross section is shown in figure 1*b*. Related procedures have also been reported for AlInGaP μ-ILEDs (Kim *et al.* 2010).

The thermal properties of devices with this type of layout are critically important because excessive heating can limit the stability, reliability and efficiency. Changes in temperature can be even more important for applications of μ-ILEDs in biology, where even modest levels of heating can induce adverse responses. Our objective was to study the thermal properties of μ-ILEDs using analytical and rigorous finite-element methods and provide simple expressions for calculating the device temperatures in terms of the material and geometry parameters. Unlike the accurate analysis (Kim *et al.* 2011) in which a very complex expression for μ-ILED temperature is given, a simple scaling law for μ-ILED temperature is derived in this paper for convenient designing of μ-ILED layout to minimize the adverse thermal effects.

2. Heat transfer model for the μ-ILED system

The thickness of a typical μ-ILED (5 μm or less) is smaller than its in-plane size L ($100 \times 100\,\mu m$) such that heat transfer occurs mainly through the top and bottom surfaces. As shown in figure 1*c*, the μ-ILED is modelled as a planar heat source with the input power Q at the BCB–glass interface. The metal interconnect of thickness H_m is on top of the BCB. The thicknesses of the BCB layer and glass substrate are H_B and H_g, respectively. Their corresponding thermal conductivities are k_m, k_B and k_g. The ambient temperature is T_0.

For simplicity, an axisymmetric model is adopted to obtain the analytical solution. The heat source is modelled as a circular disc of radius $r_0 = L/\sqrt{\pi}$ such that its area is the same as that (L^2) of the μ-ILED. Such an

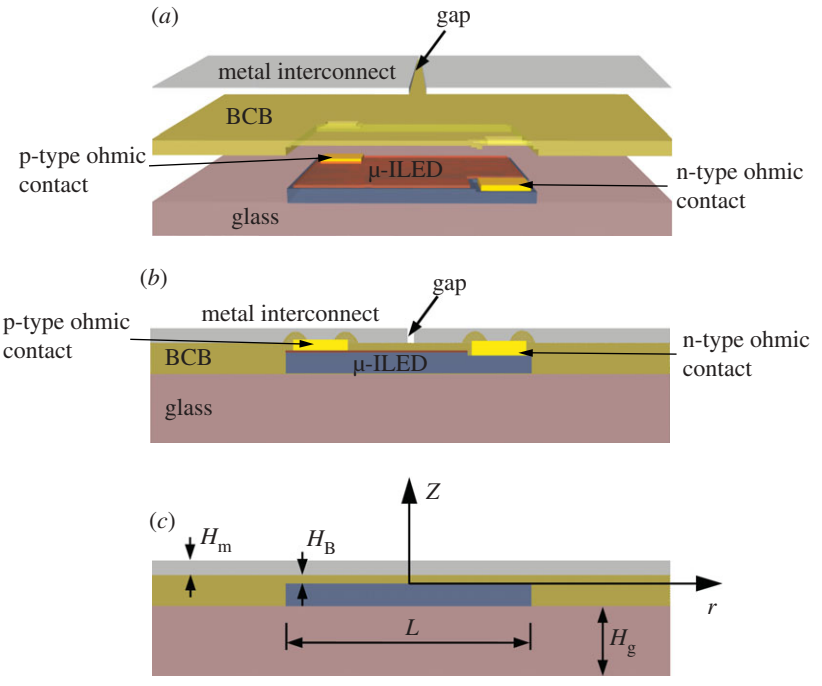

Figure 1. A schematic of the μ-ILED structure: (*a*) three-dimensional and (*b*) cross-sectional illustrations for experiments; and (*c*) theoretical model. (Online version in colour.)

assumption, as validated by a three-dimensional finite-element analysis (FEA) and experiments for rectangular μ-ILEDs, significantly simplifies the analysis and enables analytical solutions. The steady-state heat conduction equation is

$$\frac{\partial^2 \Delta T}{\partial r^2} + \frac{1}{r}\frac{\partial \Delta T}{\partial r} + \frac{\partial^2 \Delta T}{\partial z^2} = 0, \tag{2.1}$$

where $\Delta T = T - T_0$ is the difference between temperature T and the ambient temperature T_0, and (r, z) are the cylindrical coordinates with the origin at the centre of the heat source (figure 1*c*). Because the in-plane dimensions (approx. 50×50 mm) of the glass substrate, BCB and metal are much larger than the μ-ILED size (100×100 μm), the axisymmetric model is taken as infinity in the r direction. The natural convection condition at the top surface of the metal is

$$-k_m \frac{\partial \Delta T}{\partial z} = h \Delta T \quad \text{at } z = H_B + H_m, \tag{2.2}$$

where h is the coefficient of heat convection. The ambient temperature at the bottom surface of the glass substrate as well as the remote boundary (of metal, BCB and glass) gives

$$\Delta T = 0 \quad \text{at } z = -H_g \tag{2.3}$$

and

$$\Delta T|_{r \to \infty} = 0 \quad \text{for all } z. \tag{2.4}$$

Continuity of temperature and heat flux across the metal–BCB interface ($z = H_B$) requires

$$\Delta T|_{z=H_{B+}} = \Delta T|_{z=H_{B-}} \quad \text{and} \quad -k_m \left.\frac{\partial \Delta T}{\partial z}\right|_{z=H_{B+}} = -k_B \left.\frac{\partial \Delta T}{\partial z}\right|_{z=H_{B-}}. \tag{2.5}$$

Across the BCB–glass interface ($z = 0$), the temperature is continuous

$$\Delta T|_{z=0+} = \Delta T|_{z=0-}. \tag{2.6a}$$

The heat flux outside the μ-ILED ($r > r_0$, $z = 0$) is also continuous, which, together with the heat source condition inside the μ-ILED ($r \le r_0$, $z = 0$), gives

$$-k_B \left.\frac{\partial \Delta T}{\partial z}\right|_{z=0+} + k_g \left.\frac{\partial \Delta T}{\partial z}\right|_{z=0-} = \begin{cases} 0, & r > r_0, \\ \dfrac{Q}{\pi r_0^2}, & 0 \le r \le r_0. \end{cases} \tag{2.6b}$$

The Hankel transform $\Delta \bar{T}(\xi, z) = \int_0^\infty \Delta T(r, z) J_0(\xi r) r \, \mathrm{d}r$ (Carslaw & Jaeger 1959) of the steady-state heat conduction equation (2.1) gives the following ordinary differential equation:

$$\frac{\mathrm{d}^2 \Delta \bar{T}}{\mathrm{d}z^2} - \xi^2 \Delta \bar{T} = 0, \tag{2.7}$$

where J_0 is the 0th-order Bessel function of the first kind. This equation has the solution

$$\Delta \bar{T}(\xi, z) = A(\xi) \mathrm{e}^{-\xi z} + B(\xi) \mathrm{e}^{\xi z}, \tag{2.8}$$

where the functions $A(\xi)$ and $B(\xi)$ are A_m and B_m for metal, A_B and B_B for BCB, and A_g and B_g for the glass substrate, respectively. The Hankel transform of the boundary and continuity conditions (2.2), (2.3), (2.5) and (2.6) gives

$$-k_m \frac{\partial \Delta \bar{T}}{\partial z} = h \Delta \bar{T} \quad \text{at } z = H_B + H_m, \tag{2.9}$$

$$\Delta \bar{T} = 0 \quad \text{at } z = -H_g, \tag{2.10}$$

$$\Delta \bar{T}|_{z=H_{B+}} = \Delta \bar{T}|_{z=H_{B-}} \quad \text{and} \quad -k_m \left.\frac{\partial \Delta \bar{T}}{\partial z}\right|_{z=H_{B+}} = -k_B \left.\frac{\partial \Delta \bar{T}}{\partial z}\right|_{z=H_{B-}} \tag{2.11}$$

$$\text{and} \quad \Delta \bar{T}|_{z=0+} = \Delta \bar{T}|_{z=0-} \quad \text{and} \quad -k_B \left.\frac{\partial \Delta \bar{T}}{\partial z}\right|_{z=0+} + k_g \left.\frac{\partial \Delta \bar{T}}{\partial z}\right|_{z=0-} = \frac{Q}{\pi r_0} \frac{J_1(\xi r_0)}{\xi}, \tag{2.12}$$

where J_1 is the first-order Bessel function of the first kind.

Substitution of (2.8) into (2.9)–(2.12) gives

$$A_g = \frac{Q}{\pi r_0 k_B} \frac{J_1(\xi r_0)}{\xi^2} \alpha(\xi) \quad \text{and} \quad B_g = -\frac{Q}{\pi r_0 k_B} \frac{J_1(\xi r_0)}{\xi^2} \alpha(\xi) \mathrm{e}^{2\xi H_g} \tag{2.13}$$

for the glass substrate,

$$A_B = \bar{A}_B \frac{Q}{2\pi r_0 k_B} \frac{J_1(\xi r_0)}{\xi^2} \quad \text{and} \quad B_B = \bar{B}_B \frac{Q}{2\pi r_0 k_B} \frac{J_1(\xi r_0)}{\xi^2} \tag{2.14}$$

for the BCB layer and

$$\left.\begin{aligned} A_{\mathrm{m}} &= \left[\left(1+\frac{k_{\mathrm{b}}}{k_{\mathrm{m}}}\right)\bar{A}_{\mathrm{B}} + \left(1-\frac{k_{\mathrm{b}}}{k_{\mathrm{m}}}\right)\mathrm{e}^{2\xi H_{\mathrm{b}}}\bar{B}_{\mathrm{B}}\right]\frac{Q}{4\pi r_0 k_{\mathrm{B}}}\frac{J_1(\xi r_0)}{\xi^2} \\ \text{and} \qquad B_{\mathrm{m}} &= \left[\left(1-\frac{k_{\mathrm{b}}}{k_{\mathrm{m}}}\right)\mathrm{e}^{-2\xi H_{\mathrm{b}}}\bar{A}_{\mathrm{B}} + \left(1+\frac{k_{\mathrm{b}}}{k_{\mathrm{m}}}\right)\bar{B}_{\mathrm{B}}\right]\frac{Q}{4\pi r_0 k_{\mathrm{B}}}\frac{J_1(\xi r_0)}{\xi^2} \end{aligned}\right\} \tag{2.15}$$

for the metal layer, where

$$\bar{A}_{\mathrm{B}} = \left[\left(1+\frac{k_{\mathrm{g}}}{k_{\mathrm{B}}}\right) - \left(1-\frac{k_{\mathrm{g}}}{k_{\mathrm{B}}}\right)\mathrm{e}^{2\xi H_{\mathrm{g}}}\right]\alpha(\xi) + 1,$$

$$\bar{B}_{\mathrm{B}} = \left[\left(1-\frac{k_{\mathrm{g}}}{k_{\mathrm{B}}}\right) - \left(1+\frac{k_{\mathrm{g}}}{k_{\mathrm{B}}}\right)\mathrm{e}^{2\xi H_{\mathrm{g}}}\right]\alpha(\xi) - 1,$$

$$\alpha(\xi) = \frac{\kappa+1}{[(1-k_{\mathrm{g}}/k_{\mathrm{B}}) - (1+k_{\mathrm{g}}/k_{\mathrm{B}})\kappa] - [(1+k_{\mathrm{g}}/k_{\mathrm{B}}) - (1-k_{\mathrm{g}}/k_{\mathrm{B}})\kappa]\mathrm{e}^{2\xi H_{\mathrm{g}}}}$$

and

$$\kappa = \frac{(1-k_{\mathrm{B}}/k_{\mathrm{m}}) - (1+k_{\mathrm{B}}/k_{\mathrm{m}})((k_{\mathrm{m}}\xi-h)/(k_{\mathrm{m}}\xi+h))\mathrm{e}^{-2\xi H_{\mathrm{m}}}}{(1-k_{\mathrm{B}}/k_{\mathrm{m}})((k_{\mathrm{m}}\xi-h)/(k_{\mathrm{m}}\xi+h))\mathrm{e}^{-2\xi H_{\mathrm{m}}} - (1+k_{\mathrm{B}}/k_{\mathrm{m}})}\mathrm{e}^{-2\xi H_{\mathrm{B}}}.$$

The inverse Hankel transform $\Delta T(r,z) = \int_0^\infty \Delta\bar{T}(\xi,z)J_0(\xi r)\xi\,\mathrm{d}\xi$ then gives the temperature distributions $\Delta T_g(r,z)$, $\Delta T_B(r,z)$ and $\Delta T_{\mathrm{m}}(r,z)$ in the glass substrate, BCB and metal layers. The temperature distribution in the μ-ILED is obtained from $\Delta T_g(r,0)$, as $\Delta T_{\mu\text{-ILED}}(r) = \int_0^\infty [A_{\mathrm{B}}(\xi) + B_{\mathrm{B}}(\xi)]J_0(\xi r)\xi\,\mathrm{d}\xi$. The temperature distribution at the metal surface is $\Delta T_{\mathrm{surface}}(r) = \Delta T_{\mathrm{m}}(r, H_{\mathrm{m}} + H_{\mathrm{B}}) = \int_0^\infty [A_{\mathrm{m}}(\xi)\mathrm{e}^{-\xi(H_{\mathrm{m}}+H_{\mathrm{B}})} + B_{\mathrm{m}}(\xi)\mathrm{e}^{\xi(H_{\mathrm{m}}+H_{\mathrm{B}})}]J_0(\xi r)\xi\,\mathrm{d}\xi$, which can be rewritten to obtain the surface temperature

$$\begin{aligned} T_{\mathrm{surface}} &= T_0 + \frac{K_{\mathrm{m}}Q}{\pi k_{\mathrm{B}} r_0}\int_0^\infty \left\{\begin{aligned}&[1-(k_{\mathrm{g}}/k_{\mathrm{B}})\coth(\xi H_{\mathrm{g}})\beta(\xi)][(k_{\mathrm{B}}/k_{\mathrm{m}})\cosh(\xi H_{\mathrm{g}}) - \sinh(\xi H_{\mathrm{g}})] \\ &-[(k_{\mathrm{B}}/k_{\mathrm{m}})\sinh(\xi H_{\mathrm{g}}) - \cosh(\xi H_{\mathrm{g}})]\beta(\xi_{\mathrm{g}})\end{aligned}\right\} \\ &\quad\times \frac{e^{-\xi H_{\mathrm{m}}}}{k_{\mathrm{m}}\xi + h}J_1(\xi r_0)J_0(\xi r)\,\mathrm{d}\xi, \end{aligned} \tag{2.16}$$

where

$$\beta(\xi) = \left[\frac{(k_{\mathrm{B}}/k_{\mathrm{m}})h\tanh(\xi H_{\mathrm{B}})\tanh(\xi H_{\mathrm{m}}) + k_{\mathrm{B}}\xi\tanh(\xi H_{\mathrm{B}}) + k_{\mathrm{m}}\xi\tanh(\xi H_{\mathrm{m}}) + h}{(k_{\mathrm{B}}/k_{\mathrm{m}})h\tanh(\xi H_{\mathrm{m}}) + k_{\mathrm{B}}\xi + k_{\mathrm{m}}\xi\tanh(\xi H_{\mathrm{B}})\tanh(\xi H_{\mathrm{m}}) + h\tanh(\xi H_{\mathrm{B}})} + \frac{k_{\mathrm{g}}}{k_{\mathrm{B}}}\coth(\xi H_{\mathrm{g}})\right]^{-1}.$$

A three-dimensional FEA is used to study the temperature distributions in the metal, BCB, μ-ILED and glass. The μ-ILED ($100\times100\times50\,\mu\mathrm{m}$) is enveloped by a layer of BCB, with a total thickness of $6\,\mu\mathrm{m}$, and is modelled as a three-dimensional volume heat source with the total input power Q. The thicknesses of the metal and glass are the same as those used in the analytical model.

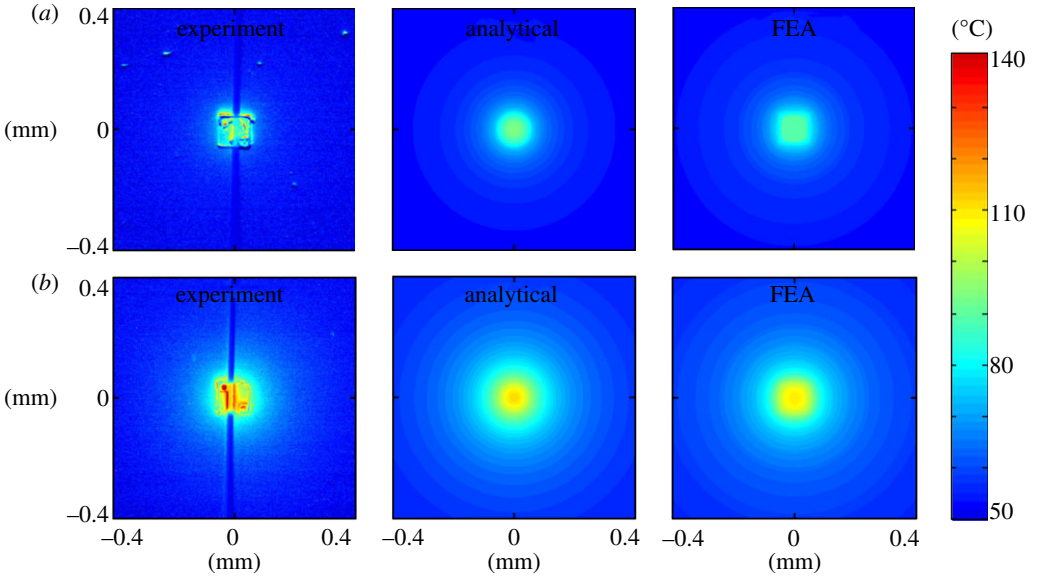

Figure 2. Surface temperature distribution given by the experiments, analytical model and FEA for (*a*) input power $Q = 12\,\mathrm{mW}$ and thickness of metal interconnect $H_\mathrm{m} = 300\,\mathrm{nm}$; and (*b*) $Q = 37.6\,\mathrm{mW}$ and $H_\mathrm{m} = 1000\,\mathrm{nm}$. (Online version in colour.)

The in-plane dimensions of the metal, BCB and glass are taken from the experiments ($50 \times 50\,\mathrm{mm}$) (Kim *et al.* 2011). The metal layer is subjected to natural convection with the ambient temperature T_0 at the top surface, while the lateral surfaces of the metal, BCB and glass, together with the bottom surface of the glass, are at a constant temperature T_0. The continuum element DC3D8 in the ABAQUS package (see ABAQUS 2009) is used in the FEA.

Figure 2 compares the surface temperature distribution in equation (2.16) with the experiments and three-dimensional FEA, which accurately accounts for the square-shaped μ-ILED with finite thickness, for the input power $Q = 12\,\mathrm{mW}$ (figure 2*a*) and $Q = 37.6\,\mathrm{mW}$ (figure 2*b*) used in the experiments, the μ-ILED size $L = 100\,\mu\mathrm{m}$ ($r_0 = 56.4\,\mu\mathrm{m}$) and ambient temperature $T_0 = 50°\mathrm{C}$. The thermal conductivity and thickness are $k_\mathrm{g} = 1.1\,\mathrm{W\,m^{-1}\,K^{-1}}$ (Lee & Cahill 1997) and $H_\mathrm{g} = 800\,\mu\mathrm{m}$ for glass, $k_\mathrm{B} = 0.3\,\mathrm{W\,m^{-1}\,K^{-1}}$ (Christiaens *et al.* 2005) and $H_\mathrm{B} = 1\,\mu\mathrm{m}$ for BCB, and $k_\mathrm{m} = 70$ and $160\,\mathrm{W\,m^{-1}\,K^{-1}}$ for the 300 and 1000 nm thick aluminium interconnects, respectively, because of their thickness-dependent thermal conductivity (La Spina *et al.* 2006; Stojanovic *et al.* 2007; Bourgoin *et al.* 2010; Schmid *et al.* 2010). The coefficient of heat convection is $h = 25\,\mathrm{W\,m^{-2}\,K^{-1}}$. The analytical model agrees well with the FEA, and both agree well with the experiment, except along the gap (shown in the left two experimental images in figure 2, and also in figure 1*a*). This is because the surface temperature at the gap in the experiments is the temperature at the next (BCB) layer, which is very close to the μ-ILED temperature because the BCB layer directly above the μ-ILED is very thin (figure 1*a*). The μ-ILED temperature is approximately the same as the surface temperature at the gap.

3. Simple scaling law for thermal management

The FEA suggests that the temperature in the μ-ILED is very uniform except near its small side surfaces. This is because the in-plane size of the μ-ILED (L) is much larger than its thickness such that heat transfer from the μ-ILED occurs mainly through its top and bottom surfaces. The temperature increase in the μ-ILED can then be obtained analytically by averaging the temperature at the BCB–glass interface over the radius r_0 as

$$\Delta T_{\mu\text{-ILED}} = \frac{2Q}{\pi k_B r_0^2} \int_0^\infty \beta(\xi) J_1^2(\xi r_0) \frac{\mathrm{d}\xi}{\xi^2}. \tag{3.1}$$

Both the analytical model and FEA suggest that the natural convection at the top surface of the metal interconnect has a negligible effect on the temperature in the μ-ILED. The thick glass substrate ($H_g \gg H_m$, H_B, r_0) can be modelled as a semi-infinite solid. These, together with the low thermal conductivity of BCB, $k_B \ll k_m$, simplify equation (3.1) to

$$\Delta T_{\mu\text{-ILED}} = \frac{2Q}{\pi k_B r_0} \int_0^\infty \left[\frac{k_m \tanh(H_m x/r_0)}{k_B + k_m \tanh(H_B x/r_0) \tanh(H_m x/r_0)} + \frac{k_g}{k_B} \right]^{-1} J_1^2(x) \frac{\mathrm{d}x}{x^2}. \tag{3.2}$$

For a μ-ILED with size much larger than the metal and BCB layer thickness ($r_0 \gg H_m$, H_B), $\tanh(H_m x/r_0) \sim H_m x/r_0$ and $\tanh(H_B x/r_0) \sim H_B x/r_0$ (and $J_1^2(x)x^{-2}$ in the integrand decreases rapidly with x), expression (3.2) can be further simplified to

$$\Delta T_{\mu\text{-ILED}} = \frac{2Q}{\pi k_m H_m} \int_0^\infty \frac{1 + ((k_m H_m/k_g r_0)(k_g H_B/k_B r_0))x^2}{x + ((k_g r_0/k_m H_m) + (k_g H_B/k_B r_0))x^2} J_1^2(x) \frac{\mathrm{d}x}{x^2}. \tag{3.3}$$

It gives a simple scaling law such that the normalized temperature increase $k_m H_m \Delta T_{\mu-\text{ILED}}/Q$ in the μ-ILED depends on only two combinations of material and geometry parameters: the normalized μ-ILED size $k_g r_0/(k_m H_m)$ and the BCB layer thickness $k_g H_B/(k_B r_0)$. The latter is very small ($k_g H_B/(k_B r_0) \ll 1$) because $r_0 \gg H_B$ and the thermal conductivities of the BCB and glass are of the same order of magnitude. Numerical integrations suggest that $[k_g H_B/(k_B r_0)]x^2$ can be neglected in equation (3.3) (also because $J_1^2(x)x^{-2}$ decreases rapidly with x). This leads to a simple, analytical expression for the temperature in the μ-ILED,

$$\Delta T_{\mu\text{-ILED}} = \frac{2Q}{\pi k_m H_m} \int_0^\infty \left(x + \frac{k_g r_0}{k_m H_m} \right)^{-1} J_1^2(x) \frac{\mathrm{d}x}{x^2}. \tag{3.4}$$

The normalized temperature increase $k_m H_m \Delta T_{\mu\text{-ILED}}/Q$ in the μ-ILED depends only on the normalized radius $k_g r_0/(k_m H_m)$. It is independent of the BCB property and thickness because the BCB layer is very thin and has low thermal conductivity. This simple expression agrees very well with the accurate solution in

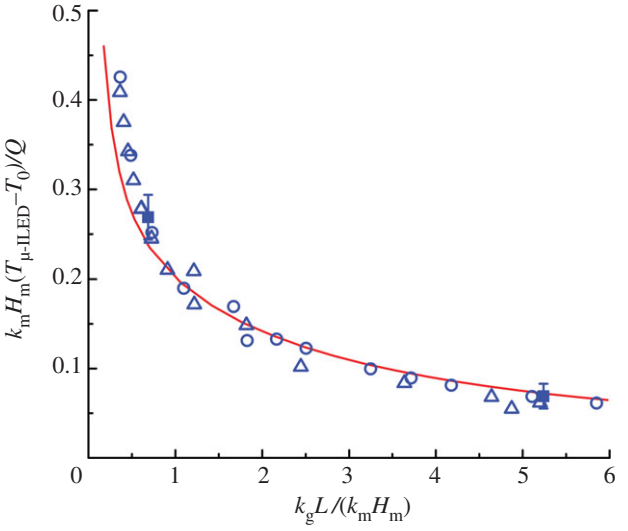

Figure 3. The normalized temperature increase in the μ-ILED versus the normalized μ-ILED size for the approximate solution (solid line), accurate solution (circles), FEA (triangles) and experiments (squares). (Online version in colour.)

equation (3.1) and the FEA, within a few per cent of error. Numerical integration in equation (3.4) gives an approximate but simple and explicit expression of temperature in the μ-ILED as

$$T_{\mu\text{-ILED}} \approx 0.451\frac{Q}{k_g L}\left\{1-0.842\left(\frac{k_g L}{k_m H_m}\right)^{-1}\left[1-\exp\left(-1.07\frac{k_g L}{k_m H_m}\right)\right]\right\}+T_0, \tag{3.5}$$

where the μ-ILED size L has substituted $\sqrt{\pi}r_0$, and the first two terms $0.451Q(k_gL)^{-1}\{1-0.842[k_gL/(k_mH_m)]^{-1}\}$ on the right-hand side result from the asymptotic analysis of equation (3.4) for relatively large $k_gL/(k_mH_m)$. The temperature increase $(T_{\mu\text{-ILED}}-T_0)$ obtained from equation (3.5) is only a few per cent different from that given by equation (3.4). Figure 3 shows the normalized temperature increase in the μ-ILED versus the normalized μ-ILED size. The solid line is for the approximate solution in equation (3.5), while the accurate solution in equation (3.1), three-dimensional FEA and experiments are also shown. Their excellent agreement validates the analytical expression for the temperature in the μ-ILED in equation (3.5). This equation can serve as a guideline for the thermal management design of μ-ILEDs by selecting metal interconnects to minimize the adverse thermal effects. It suggests that thick metal interconnects or their large thermal conductivity will be effective in dissipating heat in μ-ILEDs. The scaling law in equation (3.5) (also shown in figure 3) indicates that the increase in μ-ILED size or the substrate thermal conductivity, for a given input power, also decreases the temperature in μ-ILEDs.

4. Conclusion

In conclusion, we have developed an analytical model to study the thermal properties of μ-ILEDs. The agreement between the predicted surface and μ-ILED temperatures with experiments and finite-element simulations validates the analytical model. We further approximate the μ-ILED temperature in terms of one combination of material and geometry parameters. Although the heat transfer in the current μ-ILED system should be in a three-dimensional manner, for which a solution for three-dimensional heat transfer in Cartesian coordinates is also obtainable, it is almost impossible to derive a simple scaling law such as equation (3.5). Such a simple analytical expression is very useful in the design of the μ-ILED layout to reduce the thermal effects on the performance of μ-ILEDs. The model in this paper can be easily extended to study other μ-ILED systems with other layouts and materials, for different types of applications.

C.L. acknowledges support from the NSFC (grant no. 11172263) and the New Star Program from Zhejiang University. C.L. and Y.L. acknowledge support from the CSC. J.Z., Y.H. and J.A.R. acknowledge support from the NSF (OISE-1043161, 1043143 and 1043135). Y.H. also acknowledges support from the NSFC.

References

ABAQUS. 2009 *Analysis user's manual v.6.9.* Pawtucket, RI: Dassault Systèmes.

Bourgoin, J. P., Allogho, G. G. & Hache, A. 2010 Thermal conduction in thin films measured by optical surface thermal lensing. *J. Appl. Phys.* **108**, 073520. (doi:10.1063/1.3490185)

Carslaw, H. S. & Jaeger, J. C. 1959 *Conduction of heat in solids*, 2nd edn. Oxford, UK: The Clarendon Press.

Christiaens, I., Roelkens, G., Mesel, K. D., Thourhout, D. V. & Baets, R. 2005 Thin-film devices fabricated with benzocyclobutene adhesive wafer bonding. *J. Lightwave Technol.* **23**, 517–523. (doi:10.1109/JLT.2004.841783)

Kim, R. H. *et al.* 2010 Waterproof AlInGaP optoelectronics on stretchable substrates with applications in biomedicine and robotics. *Nat. Mater.* **9**, 929–937. (doi:10.1038/nmat2879)

Kim, H. S. *et al.* 2011 Unusual strategies for using indium gallium nitride grown on silicon (111) for solid-state lighting. *Proc. Natl Acad. Sci. USA* **108**, 10 072–10 077. (doi:10.1073/pnas.1102650108)

La Spina, L., Nenadovic, N., van Herwaarden, A. W., Schellevis, H., Wien, W. H. A. & Nanver, L. K. 2006 MEMS test structure for measuring thermal conductivity of thin films. In *Proc. of the 2006 IEEE Int. Conf. on Microelectronics Test Structures* (*ICMTS 2006*), Austin, TX, 6–9 March 2006, pp. 137–142.

Lee, S. M. & Cahill, D. G. 1997 Heat transport in thin dielectric films. *J. Appl. Phys.* **81**, 2590–2595. (doi:10.1063/1.363923)

Schmid, A. J., Cheaito, R. & Chiesa, M. 2010 Characterization of thin metal films via frequency-domain thermoreflectance. *J. Appl. Phys.* **107**, 024908. (doi:10.1063/1.3289907)

Schubert, E. F. & Kim, J. K. 2005 Solid-state light sources getting smart. *Science* **308**, 1274–1278. (doi:10.1126/science.1108712)

Stojanovic, N., Yun, J. S., Washington, E. B. K., Berg, J. M., Holtz, M. W. & Temkin, H. 2007 Thin-film thermal conductivity measurement using microelectrothermal test structures and finite-element-model-based data analysis. *J. Microelectromech. Syst.* **16**, 1269–1275. (doi:10.1109/JMEMS.2007.900877)

Tsao, J. Y., Coltrin, M. E., Crawford, M. H. & Simmons, J. A. 2010 Solid-state lighting: an integrated human factors, technology, and economic perspective. *Proc. IEEE* **98**, 1162–1179. (doi:10.1109/JPROC.2009.2031669)